13.10

# CLOUD-RESOLVING NUMERICAL SIMULATION OF A POLAR LOW OVER THE JAPAN SEA

**Wataru Yanase*, Hiroshi Niino**
**Ocean Research Institute, University of Tokyo, Tokyo, Japan**
**and**
**Kazuo Saito**
**Meteorological Research Institute, Ibaraki, Japan**

## 1. INTRODUCTION

In cold seasons, satellite imagery often shows meso-$\alpha$-scale lows developing over high-latitude oceans in the polar side of a polar front. They are called "polar lows" (Harley, 1960). Some of them look like miniature extratropical cyclones having a comma-like cloud pattern, while the others resemble tropical cyclones having a cloud-free eye and spiral cloud bands. Because of their appearance, their developing mechanisms have recieved considerable attention by atmospheric scientists. These lows have been also socially important: In Japan, they not only bring heavy snowfall over the coast of the Japan Sea, but also cause disasters such as shipwrecks.

In spite of their social and meteorological importance, however, their detailed structures are not well known since they form over data sparse regions such as high-latitude oceans in winter. There have been a few high-resolution observations of a polar low (Shapiro *et al.*, 1987; Hewson *et al.*, 2000). Even in these observations, however, the number of observed physical variables have been considerlably limited. Recent developments in computer technology and meso-scale numerical modelling suggest that a numerical simulation may be a promising tool to reproduce a realistic polar low. Using a non-hydrostatic model with 5-km horizontal grid interval, Fu (1999) succeeded to simulate a remarkable polar low with a cloud-free eye that developed over the Japan Sea. In order to represent realistically individual cumulus convections and their organization processes that play an important role in a polar low, however, even higher resolution seems to be required. In the first part of this study, we will report the structure of a polar low as revealed from a cloud-resolving simulation using a non-hydrostatic model with 2-km horizontal grid interval.

* Corresponding author address: Wataru Yanase, Ocean Research Institute, Univ. of Tokyo, Tokyo 164-8639, Japan; e-mail: yanase@ori.u-tokyo.ac.jp.

Formation and development mechanisms of polar lows are also not well clarified. Several mechanisms have been suggested: Baroclinic instability, forcing of the upper cold vortex, CISK (Charney and Eliassen, 1964) and WISHE (Emanuel and Rotunno, 1989). These mechanisms seem to operate with different importance depending on cases, regions and stages, and some of them may operate simultaneously. In order to investigate these complicated mechanisms, sensitivity experiments have been made (Sardie and Warner, 1985; Bresch *et al.*, 1997). One of the difficulties in the sensitivity experiment, however, is that a switching on/off a certain physical process affects not only the vortex but also its environment. Thus, it becomes difficult to judge whether the deformation of the environment changes the vortex behavior or the vortex itself is deformed. In order to avoid this problem, we have made improved sensitivity experiments to clarify the development mechanism.

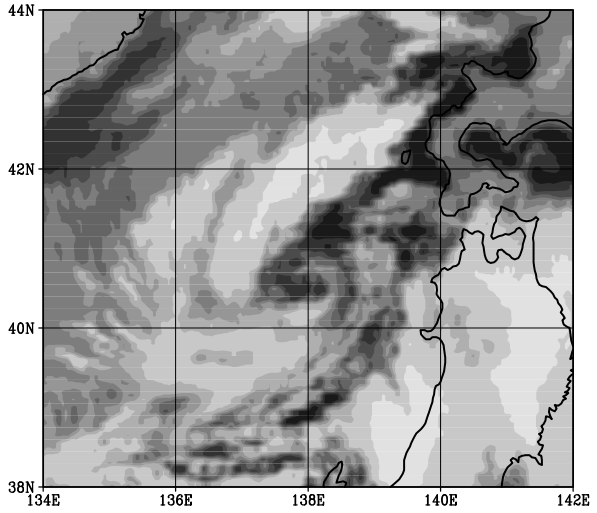


Figure 1: GMS-5 IR image of the polar low at developing stage at 16 UTC 21 January 1997. The low center is located at 138°E, 40.5°N.

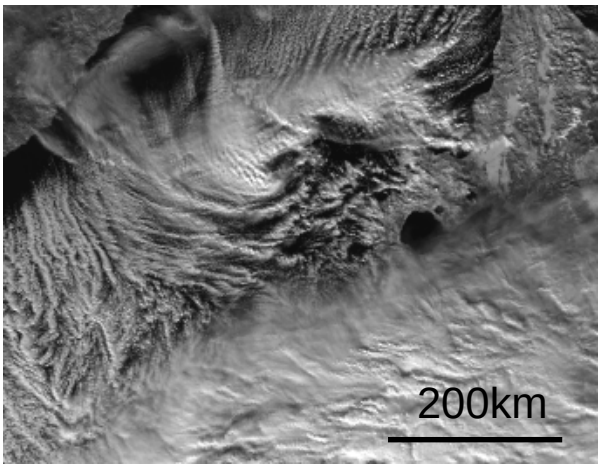


Figure 2: NOAA VIS image at 0408 ~ 0421 UTC 21 January 1997. The polar low is developing off the west coast of Hokkaido island. Cloud streets accompanying polar airmass outbreak are seen to the west and north of the polar low at initial stage.

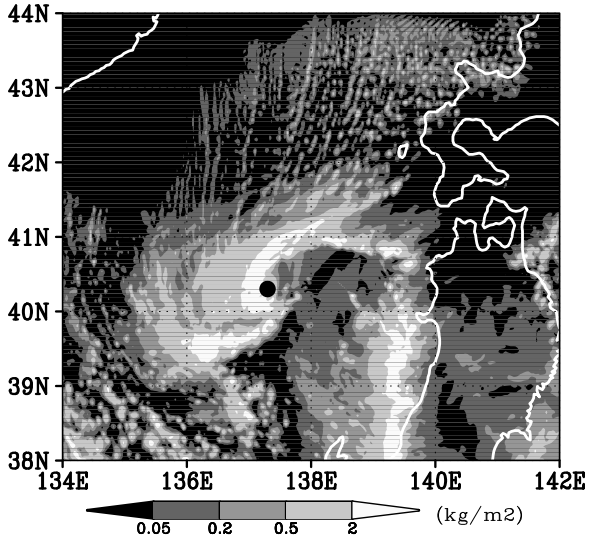


Figure 3: Simulated vertically-integrated total liquid and solid water at 16 UTC 21 January 1997. The solid circle denotes the low center defined by the sea level pressure.

## 2. CLOUD-RESOLVING SIMULATION

On 21 January 1997, a remarkable polar low with a cloud-free eye and spiral cloud bands developed over the Japan Sea (Fig.1). This polar low formed off the west coast of Hokkaido island within the polar air outbreak from the Asian continent (Fig.2). A parallel version of MRI-NHM (Meteorological Research Institute Non-Hydrostatic Model; Saito *et al.* 1999) is used for the simulation. The model considers short and long wave radiations (Yamamoto and Satomura, 1994), surface heat balance (Kondo, 1975), sub-grid turbulence (Klemp and Wilhelmson, 1978) and cold rain microphysics with mixing ratios of water vapor, cloud water, rain, cloud ice, snow and graupel as prognostic variables. The size of the calculation domain is 720 km × 720km in the horizontal direction and about 19 km in the vertical direction. The horizontal grid spacing is 2km, which is capable of marginally resolving cumulus convections. The vertical grid interval is varied from 40 m near the ground to about 1000 m near the top of the calculation domain. The time integration was started from 0000 UTC 21 January and continued for 24 hours. The initial and boundary conditions were taken from the 24-hours prediction of RSM (Regional Spectral Model; a primitive equation model for routine numerical prediction of Japan Meteorological Society; Nakamura, 1995) starting from 0000 UTC 21 January.

Figure 3 shows the vertically-integrated total liquid and solid water (sum of cloud water, rain, cloud ice, snow and graupel) at 16 UTC, when the polar low was well organized. Observed features of the polar low such as the spiral bands, the cloud-free eye and the cloudy region in the west of the low (Fig. 1) are successfully reproduced. In addition, cloud streets around the polar low are also well reproduced (cf. Fig.2; note that the time is about 04 UTC).

Figure 4 shows the total liquid and solid water in zonal-vertical cross section across the low center (40.3°N, 137.3°E) at 16 UTC 21. In the west of the low, the total liquid and solid water extends to the height of about 5 km. In the east of the low, on the other hand, little total liquid and solid water exist.

In order to understand the formation mechanism of the cloudy region in the west of the low and cloud-free eye, the hight of 265K equivalent potential temperature surface and the vortex-relative horizontal wind vector on the surface are plotted in Fig. 5. In the northern side of the spiral band to the northeast of the low center, the vortex-relative wind is easterly and the heights of the equivalent potential temperature increases toward west, indicating that the air in the northeast of the low ascends as it moves cyclonically to the west of the low center. This ascending motion causes the cloudy region in the west of the low. In the southern side, on the other hand, the

vortex-relative wind is southerly and the height of the equivalent potential temperature decreases toward northeast. Thus, the air descends as it moves eastward cyclonically toward the low center. This explains cloud-free region from the low center to the east (Fig.1). This is also consistent with the Fu(1999)'s finding that the warm core structure near the cloud-free eye is caused by an adiabatic descent.

Figure 6 shows vertical vorticity and zonal-vertical wind vector in zonal-vertical cross section across the low center. The maximum vorticity of $2.9\times10^{-3}s^{-1}$ is found at about 300 m height. The axis of the strong vertical vorticity and that of the updraft are not vertical but slopes remarkably to the west with the gradient of 1/5. The mechanism for such a large slope is not known at present. It is noted, however, that tropical cyclones also have a similar sloped structure (Jorgensen, 1984; Zhang *et al.* 2001).

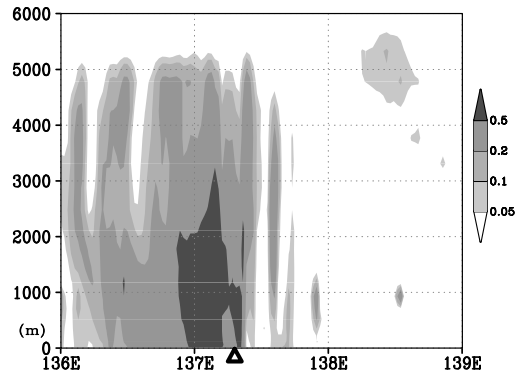


Figure 4: Total liquid and solid water in the zonal-vertical cross section across the low center at 16 UTC 21. The low center is at (40.3°N, 137.3°E) and is indicated by the triangle

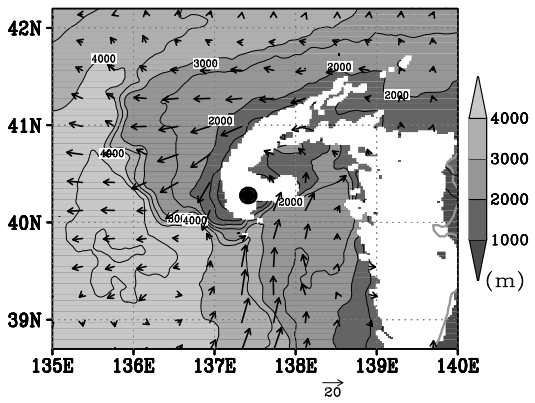


Figure 5: Height of the 265K equivalent potential temperature surface and vortex-relative horizontal wind vector on the surface at 16 UTC 21. The solid circle denotes the low center defined by the sea level pressure. White regions indicate where the 265K equivalent potential temperature surface crosses the earth's surface.

## 3. THE SENSITIVITY EXPERIMENTS

In order to investigate the developing mechanism of this polar low, its sensitivities to condensational heating and surface fluxes of sensible and latent heat have been examined. The model is nearly same as the one used in the previous section except that the horizontal grid interval is 6 km for the purpose of saving the CPU time. Note that no cumulus parameterization is used. Four experiments were performed: CONTROL (control run), DRY (no condensational heating), NOFLUX (no surface heat fluxes) and D&NF (no condensational heating and no surface heat fluxes).

Figure 7 shows time evolution of vorticities between 12 and 18 UTC after the polar low is well organized. Since NOFLUX and D&NF do not show a noticeable development, the surface heat fluxes seem to

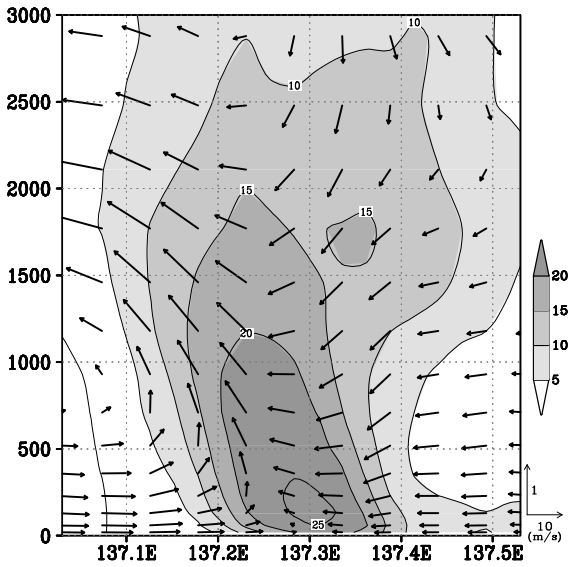


Figure 6: Vertical voriticity (in unit of $10^{-4}s^{-1}$) and zonal-vertical wind vector on zonal-vertical cross section at 40.3°N at 16 UTC 21 January.

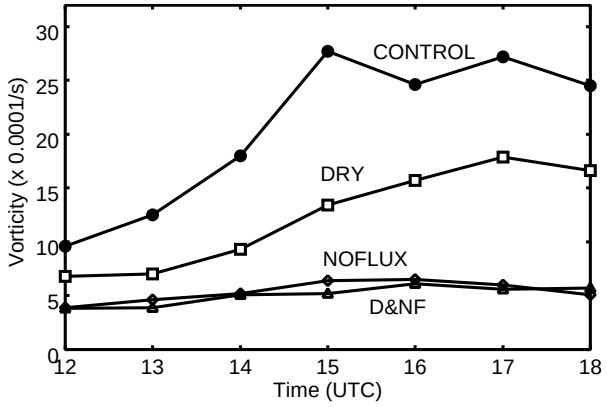


Figure 7: Time evolutions of vorticities for the 24-hour sensitivity experiments

be crucial for the vortex development. On the other hand, since DRY develops moderately, the condensational heating seems to be important to some extent.

As mentioned in the introduction, however, when physical processes are removed, not only the vortex itself but also its environment can be deformed. In fact, the vertical profiles of potential temperature in the region that is not affected by the polar low shows that a convective mixed layer does not develop in NOFLUX and D&NF (Fig. 8) Thus, in these experiments, the stratification remains stable even near the sea surface (Fig.8), so that baroclinic instability and forcing of the upper cold vortex are likely to be suppressed.

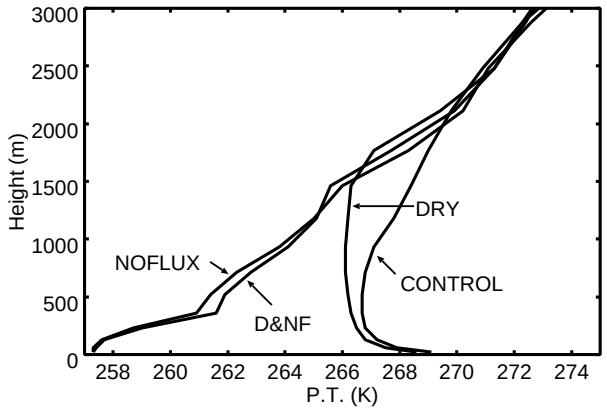


Figure 8: Vertical profile of potential temperature (K) in the environment area at 12 UTC. The polar low reaches this region 6 hours later and has not affected this area yet.

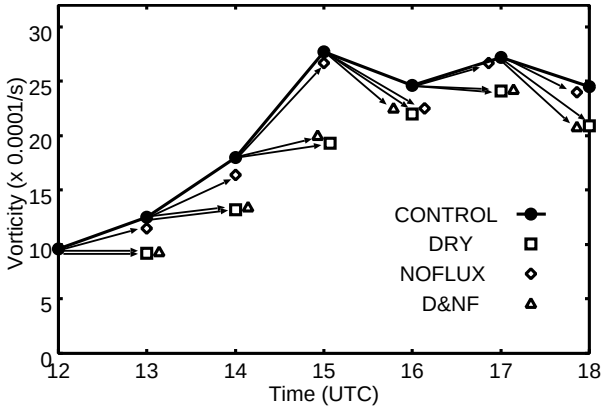


Figure 9: Time evolutions of vorticities for the 1-hour sensitivity experiments. The vorticities for the sensitivity experiment at 13 UTC, for example, are obtained by running the model for 1 hour from the initial field taken from CONTROL at 12 UTC.

In an attempt to isolate the effects of physical processes on the vortex itself from those on the vortex environment, we have made another sensitivity experiments in which time integrations with and without physical processes have been made only for an hour (Fig.9): In these sensitivity experiments, the result of CONTROL are used as the initial field. Since NOFLUX develops nearly same as CONTROL does, the surface heat fluxes do not seem to affect the vortex development within an hour. On the other hand, DRY and D&NF hardly developed. Thus, condensational heating is found to be very important for the vortex development within an hour. This result seems to contradict that of the 24-hour experiments discribed above.

The difference between the results of the 24-hour experiments and those of 1-hour experiments may be explained as follows: For the 1-hour experiments, the deformation of the environment is almost negligible. Thus, they are suitable for examining the effects of physical processes on the vortex development. Their results show that the condensational heating is primarily important for the vortex intensification, while that the surface heat fluxes are almost unimportant for the development for a short time scale. For the 24-hour experiments, on the other hand, the surface heat fluxes affects the environment significantly as shown in Fig.8. Thus, the vortex development is affected through the modification of the environment. If the modification of the environment is very large, condensational heating alone would not be capable of developing the

vortex.

## 4. SUMMARY

The structure of the polar low which formed over the Japan Sea on 21 January 1997 was studied by using the cloud-resolving non-hydrostatic model with 2-km horizontal grid interval. The observed feature of the polar low such as its movement, spiral bands, a cloud-free eye and cloud streets associated with cold air outbreak were well reproduced. The cloudy region in the north and west of the low is shown to correspond to an ascending westward flow, while the cloud-free region in the south and east of the low corresponds to a descending flow. The maximum vertical vorticity near the low center reaches as large as $2.9\times10^{-3}s^{-1}$ at 300 m height. The axis of the maximum vertical vorticity is not vertical but slopes significantly to the west with increasing height.

In order to investigate the developing mechanism of the polar low, sensitivity experiments have been performed. It is found that the condensational heating is of primary importance for the intensification of the vortex. On the other hand, surface heat fluxes are important in a sense that they maintain the environment for the vortex development.

*Acknowledgments.* The present work is partly supported by Grant-in-Aids for Scientific Research on Priority Areas (B)(2) No.12125201, the Ministry of Education, Culture, Sports, Science and Technology.

## REFERENCES

Bresch, J. F., R. J. Reed, and M. D. Algright, 1997: A polar low development over the Bering Sea: Analysis, numerical simulation, and sensitivity experiments. *Mon.Wea.Rev.*, **125**, 3109–3130.

Charney, J. and A. Eliassen, 1964: On the growth of the hurricane depression. *J. Atmos. Sci*, **21**, 68–75.

Emanuel, K. and R. J. Rotunno, 1989: Polar low as arctic hurricanes. *Tellus*, **41A**, 1–17.

Fu, G., 1999: An ovservational and numerical study on polar lows over the Japan Sea. *PhD thesis, Univ. of Tokyo*, 109pp.

Harley, D. G., 1960: Frontal contour analysis of a polar low. *Meteor. Mag.*, **89**, 146–147.

Hewson, T. D., G. C. Craig and C. Cluad, 2000: Evolution and mesoscale structure of a polar low outbreak. *Quart. J. Roy. Meteor. Soc.*, **126**, 1031–1063.

Jorgensen, D. P., 1984: Mesoscale and convective-scale characteristics of mature hurricanes. Part II: Inner core structure of hurricane Allen (1980). *J. Atmos. Sci.*, **41**, 1287–1311.

Klemp, J. B. and R. Wilhelmson, 1978: The simulation of three-dimensional convective storm dynamics. *J. Atmos. Sci.*, **35**, 1070–1096

Kondo, J., 1975: Air-sea bulk transfer coefficients in diabatic conditions. *Boundary-Layer Meteor.*, **9**, 91–112

Nakamura, M., 1995: Regional Spectral Model. *Prog. Rep. Num. Wea. Prediction.*, **28**, 47–54.

Saito, K., T. Kato, H. Eito, T. Muroi, G. Kuman, Y. Yamagishi, and T. Yonemura, 1999: The parallel version of cloud-resolving Non-Hydrostatic Model. *Preprint Fall Meeting of Meteor. Soc. Japan*, **76**, B306 (in Japanese).

Sardie, J. M., and T. T. Warner, 1983: A numerical study of the development mechanism of polar lows. *Tellus*, **37A**, 460–477.

Shapiro, M. A. and Tedor, L. S., and T. Hampel, 1987: Research aircraft measurements of a polar low over the Norwegian Sea. *Tellus*, **39A**, 272–306.

Yamamoto, A and T. Satomura, 1994: An introduction of a radiation scheme in non-hydrostatic model. *Preprint Spring Meeting of Meteor. Soc. Japan*, **65**, A103 (in Japanese).

Zhang, D. L., Y. Liu, and M. K. Yau, 2001: A multiscale numerical study of hurricane Andrew (1992). Part IV: Unbalanced Flows. *Mon.Wea.Rev*, **129**, 92–107.